Measurement of Elastic Moduli of the Arterial Wall at Multiple Frequencies by Remote Actuation for Assessment of Viscoelasticity

Hideyuki HASEGAWA* and Hiroshi KANAI

Graduate School of Engineering, Tohoku University, Sendai 980-8579, Japan

To characterize tissues in atherosclerotic plaques, we have developed a method, the *phased tracking method*, for measuring the strain (change in wall thickness) and elasticity of the arterial wall. However, some types of tissue, such as lipids and blood clots, cannot be discriminated from each other based only on elasticity due to the small difference in their elasticity. For more precise tissue characterization, we have measured the regional viscoelasticity. To obtain the viscoelasticity, in this study, elastic moduli at multiple frequencies were measured with ultrasound by generating the change in internal pressure due to remote cyclic actuation. Furthermore, the viscoelasticity of the arterial wall was estimated from the measured elastic moduli at multiple actuation frequencies.   [DOI: 10.1143/JJAP.43.3197]

1. Introduction

The steady increase in the number of patients with myocardial infarction or cerebral infarction, both of which are considered to be caused primarily by atherosclerosis, is becoming a serious problem. Therefore, it is important to diagnose atherosclerosis in the early stage. Computed tomography (CT) and magnetic resonance imaging (MRI) are employed for the diagnosis of atherosclerosis. They subject patients to physical and mental hardships, and they provide information only on the shape of the artery, such as the diameter of the lumen. However, the diameter of the lumen is not changed by early-stage atherosclerosis.[1]

Because significant differences exist between the elastic moduli of normal arterial walls and those affected by atherosclerosis,[2,3] the evaluation of the elasticity of the arterial wall is useful for the diagnosis of early-stage atherosclerosis.[4] In addition, it is also important to assess the vulnerability of the atherosclerotic plaque, because the rupture of the plaque may cause acute myocardial infarction and cerebral infarction.[5–7] The evaluation of mechanical properties, such as the elasticity of the atherosclerotic plaque, is useful for these purposes.

To obtain the circumferential distensibility of the arterial wall in the plane perpendicular to the axial direction of the artery, methods for the measurement of the change in artery diameter have been proposed.[8–12] By assuming the artery to be a cylindrical shell, the average elasticity of the entire circumference in the plane has been evaluated.[13–15] However, the regional elasticity of the atherosclerotic plaque cannot be obtained by these methods because an artery with atherosclerotic plaques cannot be assumed to be a cylindrical shell with uniform wall thickness.

To characterize the tissue in the atherosclerotic plaque, a method for the measurement of the regional elastic modulus of the arterial wall in patients with or without atherosclerotic plaques is needed. Such a technique for the measurement of the spatial distribution of the regional elasticity would be useful for the assessment of the vulnerability of the atherosclerotic plaque as well as for the diagnosis of early-stage atherosclerosis. For this purpose, we have developed a method, the *phased tracking method*, for the measurement of small changes in the thickness of the arterial wall (less than $100\,\mu m$) due to the heartbeat.[16–24] From basic experiments, the accuracy in the measurement of the change in thickness has been less than $1\,\mu m$ using the *phased tracking method*.[17,20,21] From the change in thickness measured by our method, the regional strain and the elasticity of the arterial wall can be evaluated noninvasively.[23,25]

From the measured elastic property, it should be possible to discriminate tissues in the atherosclerotic plaque, such as fibrous tissue, lipids, and calcified tissue, due to large differences in their respective elasticities. However, it is difficult to discriminate some tissues such as lipids and blood clots because of small differences in their elasticities. An additional mechanical property of tissue with the potential to provide useful information for the discrimination of tissues is viscosity.

In the methods mentioned, including our method, the elastic modulus at about 1 Hz due to heartbeat is obtained. However, it is difficult to determine the viscoelasticity from the measurement of the elastic modulus at only one frequency. To obtain the viscoelasticity, we measured the elastic moduli from changes in wall thickness at multiple frequencies generated by the change in internal pressure due
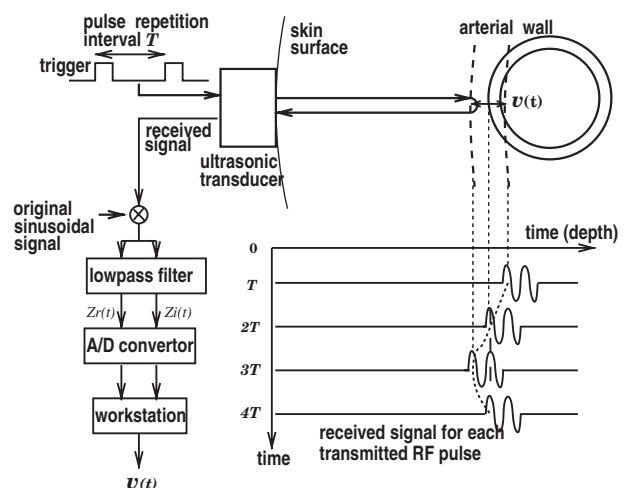

Fig. 1.   Schematic diagram of the *phased tracking method*.

*E-mail address: hasegawa@us.ecei.tohoku.ac.jp

to remote cyclic actuation.[26] The elastic modulus increased with actuation frequency.

In this study, by assuming the Voigt model as a viscoelastic model of the wall, the static elastic modulus and the viscosity constant of a silicone rubber tube are estimated from the elastic moduli measured at multiple actuation frequencies. The estimated static elastic modulus and viscosity constant are validated by comparison with those measured by a laser line gauge. Furthermore, the viscoelasticity of a human carotid artery is measured by applying remote actuation at the brachial artery.

2. Principles

2.1 Measurement of the change in wall thickness by the phased tracking method

As illustrated in Fig. 1, for the measurement of the small change in wall thickness, the phase shift of the echo caused by displacement of an object is estimated from two consecutive echoes.[16] For this purpose, quadrature demodulation is applied to the received ultrasonic waves reflected by the object and the analog-to-digital (A/D) conversion is applied to the in-phase and the quadrature signals. From the demodulated signal, $z(t; d + x(t))$, reflected at a depth $d + x(t)$ at a time t, where d and $x(t)$ are the initial depth set at $t = 0$ and the displacement of the object in the direction of the depth, the phase shift, $\Delta\phi(t)$, between two consecutive echoes is obtained from the complex cross-correlation function calculated for $M + 1$ samples in the direction of the depth as follows:

$$e^{j\Delta\hat{\phi}(t)} = \frac{\sum_{m=-M/2}^{M/2} z(t+T; d + x(t) + mD) \cdot z^*(t; d + x(t) + mD)}{\left| \sum_{m=-M/2}^{M/2} z(t+T; d + x(t) + mD) \cdot z^*(t; d + x(t) + mD) \right|}, \quad (2.1)$$

where D and T are the spacing of sample points in the depth direction and the pulse repetition interval, respectively, and $*$ represents the complex conjugate. In the measurement of the change in thickness, $M + 1$ in eq. (2.1) is set at 5 ($= 0.4\,\mu s$) in consideration of the pulse length of $0.46\,\mu s$.

From the estimated phase shift, $\Delta\hat{\phi}(t)$, the velocity, $v(t)$, of the object is obtained as follows:

$$\hat{v}(t) = -\frac{c_0}{2\omega_0} \frac{\Delta\hat{\phi}(t)}{T}, \quad (2.2)$$

where ω_0 and c_0 are the center angular frequency of the ultrasonic pulse and the speed of sound, respectively.

In the estimation of the phase shift from eq. (2.1), the position of the object is tracked by the integration of the average velocity, $v(t)$, during the pulse repetition interval, T, as follows:

$$\hat{x}(t + T) = \hat{x}(t) + \hat{v}(t) \times T$$
$$= \hat{x}(t) - \frac{c_0}{2\omega_0} \Delta\hat{\phi}(t). \quad (2.3)$$

From the displacements, $x_A(t)$ and $x_B(t)$, of two points set in the arterial wall along an ultrasonic beam, the small change in thickness, $\Delta h(t)$, between these two points is obtained as follows:

$$\Delta\hat{h}(t) = \hat{x}_A(t) - \hat{x}_B(t)$$
$$= \int_0^t \{\hat{v}_A(t) - \hat{v}_B(t)\} dt. \quad (2.4)$$

2.2 Elastic modulus obtained by measuring the change in wall thickness

From the measured change in wall thickness, the circumferential elastic modulus is obtained as follows:[23] Under *in vivo* conditions, the artery is strongly restricted in the axial direction. Therefore, a two-dimensional stress-strain relationship can be assumed.

Under such conditions, the radial incremental strain, $\Delta\varepsilon_r(t)$, which is defined by dividing the change in thickness, $\Delta h(t)$, by the thickness of wall, h_0, at the end of diastole, is expressed by the radial and circumferential incremental stresses, $\Delta\sigma_r(t)$ and $\Delta\sigma_\theta(t)$, as follows:

$$\Delta\varepsilon_r(t) = \frac{\Delta h(t)}{h_0}$$
$$= \frac{\Delta\sigma_r(t)}{E_r} - \nu\frac{\Delta\sigma_\theta(t)}{E_\theta}, \quad (2.5)$$

where E_r, E_θ, and ν are the radial and circumferential elastic moduli and Poisson's ratio, respectively.

From the change in internal pressure, $\Delta p(t)$, the circumferential and radial incremental stresses, $\Delta\sigma_r(t)$ and $\Delta\sigma_\theta(t)$, are expressed as follows:

$$\Delta\sigma_\theta(t) = \frac{r_0}{h_0} \Delta p(t), \quad (2.6)$$

$$\Delta\sigma_r(t) = -\frac{1}{2} \Delta p(t), \quad (2.7)$$

where r_0 is the inner radius at the end of diastole.

By substituting eqs. (2.6) and (2.7) into eq. (2.5), eq. (2.5) is rewritten as follows:

$$\Delta\varepsilon_r(t) = -\frac{1}{2} \frac{\Delta p(t)}{E_r} - \nu\frac{r_0}{h_0} \frac{\Delta p(t)}{E_\theta}. \quad (2.8)$$

By assuming that the arterial wall is incompressible ($\nu \approx 0.5$), eq. (2.8) can be rewritten as follows:

$$E_\theta = \frac{1}{2} \left(\frac{r_0}{h_0} + \frac{E_r}{E_\theta} \right) \frac{\Delta p(t)}{-\Delta\varepsilon_r(t)}. \quad (2.9)$$

Furthermore, by assuming isotropy ($E_r \approx E_\theta$), the elastic modulus, E_θ^h, obtained from the change in wall thickness is defined as follows:

$$E_\theta^h = \frac{1}{2}\left(\frac{r_0}{h_0}+1\right)\frac{\Delta p(t)}{-\dfrac{\Delta h(t)}{h_0}}. \qquad (2.10)$$

In the literature,[27] the E_r/E_θ of the arterial wall is reported to be 0.8. By substituting $r_0/h_0 = 4.7$ and $\Delta p(t)/\Delta\varepsilon_r(t) = 200\,\text{kPa}$ as typical values into eqs. (2.9) and (2.10), the error in E_θ^h from E_θ at $E_r/E_\theta = 0.8$ is about 3%.[23] This error is negligible.

When we describe the change in wall thickness, $\Delta h(t)$, and the change in internal pressure, $\Delta p(t)$, as complex sinusoidal functions, $\Delta h_0 \cdot e^{j(2\pi f_{ac}t-\psi)}$ and $\Delta p_0 \cdot e^{j2\pi f_{ac}t}$, at an actuation frequency, f_{ac}, eq. (2.10) can be rewritten as the complex elastic modulus as follows:

$$E_\theta^h(f_{ac}) = \frac{1}{2}\left(\frac{r_0}{h_0}+1\right)\frac{\Delta p_0}{\dfrac{\Delta h_0}{h_0}}\cdot e^{j\psi}, \qquad (2.11)$$

where Δh_0 and Δp_0 are the amplitude of the change in wall thickness and that of the change in internal pressure, respectively, and ψ is the phase difference between changes in internal pressure, $\Delta p(t)$, and wall thickness, $\Delta h(t)$.

In this paper, the absolute value, $|E_\theta^h(f_{ac})|$, of the complex elastic modulus defined by eq. (2.11) is obtained from Δh_0 and Δp_0, which are measured at each actuation frequency, f_{ac}.

2.3 Estimation of viscoelasticity using the Voigt model

In our previous study,[26] it was found that the elastic modulus, $|E_\theta^h(f_{ac})|$, increased with actuation frequency, f_{ac}. The reason for this can be thought of as follows: When we assume the Voigt model, which is illustrated in Fig. 2, as a viscoelastic model of the wall, the relationship between the stress, $\Delta\sigma(t)$, and the strain, $\Delta\varepsilon(t)$, is expressed as follows:

$$\Delta\sigma(t) = E_s \cdot \Delta\varepsilon(t) + \eta\cdot\frac{d}{dt}\Delta\varepsilon(t), \qquad (2.12)$$

where E_s and η are the static elastic modulus and the viscosity constant, respectively, and E_s and η are assumed to be unchanged by the actuation frequency, f_{ac}. In eq. (2.12), $\Delta\varepsilon(t)$ and $\Delta\sigma(t)$ correspond to $-\Delta\varepsilon_r(t) = -\Delta h(t)/h_0$ and $(r_0/h_0 + 1)\Delta p(t)/2$ in eq. (2.10), respectively.

By defining $\Delta\sigma(t) = \Delta\sigma_0 \cdot e^{j2\pi f_{ac}t}$ and $\Delta\varepsilon(t) = \Delta\varepsilon_0 \cdot e^{j(2\pi f_{ac}t-\psi)}$, eq. (2.12) can be rewritten as follows:

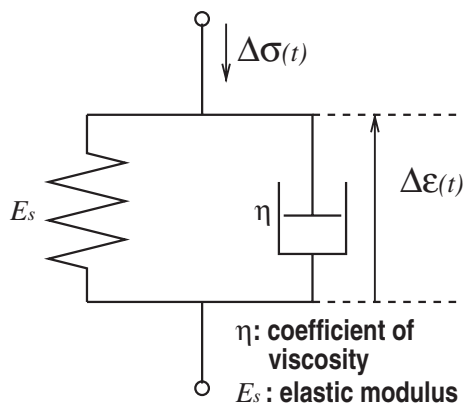$$\Delta\sigma(t) = E_s \cdot \Delta\varepsilon(t) + j2\pi f_{ac}\eta \cdot \Delta\varepsilon(t), \qquad (2.13)$$

where $\Delta\sigma_0$ and $\Delta\varepsilon_0$ are the amplitude of the stress and that of the strain, respectively.

From eq. (2.13), the complex elastic modulus, $E_{\text{Voigt}}(f_{ac}) = |E_{\text{Voigt}}(f_{ac})|e^{j\psi} = \Delta\sigma(t)/\Delta\varepsilon(t)$, is given by

$$|E_{\text{Voigt}}(f_{ac})| = \sqrt{E_s^2 + (2\pi f_{ac}\eta)^2}, \qquad (2.14)$$

$$\psi = \tan^{-1}\left(\frac{2\pi f_{ac}\eta}{E_s}\right). \qquad (2.15)$$

In eq. (2.14), the absolute value of the complex elastic modulus of the Voigt model increases with the frequency of the applied stress, and such frequency characteristics can be observed in the elastic modulus measured by ultrasound.[26] In this study, the static elastic modulus, E_s, and the viscosity constant, η, are estimated by fitting $|E_{\text{Voigt}}(f_{ac})|$ to $|E_\theta^h(f_{ac})|$ measured at multiple actuation frequencies, f_{ac}.

3. Experimental Setup

3.1 Experimental system for basic experiments

The experimental system for basic experiments using a silicone rubber tube is illustrated in Fig. 3. In this system, the change in pressure inside the silicone rubber tube is generated by compressing a rubber balloon, which is placed at a position 40 cm away from an ultrasonic probe, with an actuator. This system simulates the measurement of the change in the wall thickness of the carotid artery due to remote actuation applied at the brachial artery. The change in wall thickness due to the resulting change in internal pressure is measured using ultrasound, and the internal pressure is also measured by a pressure transducer (NEC
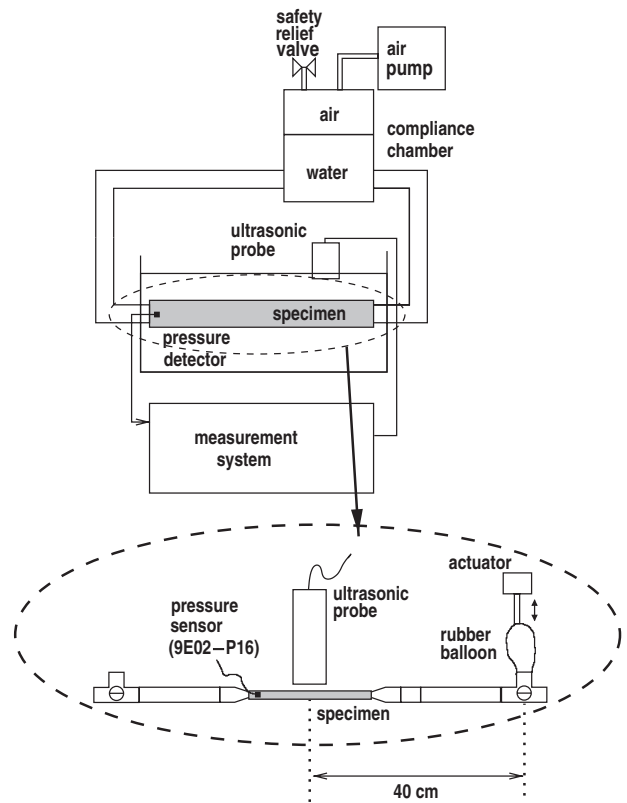

Fig. 2. Voigt model.

Fig. 3. Experimental system for basic experiments.

9E02-P16) placed inside the tube. From the measured changes in wall thickness and internal pressure, the elastic modulus can be obtained by eq. (2.11).

3.2 Measurement system

An ultrasonic pulse (center frequency: 7.5 MHz) was transmitted and received by an ultrasonic probe in standard ultrasonic diagnostic equipment (TOSHIBA SSH-140A). The signal received was amplified and demodulated. The resultant in-phase and quadrature signals were simultaneously A/D converted with a 12-bit A/D converter at a sampling frequency of 10 MHz. The measured digital signals were transfered to a computer, and the change in wall thickness was obtained by applying the *phased tracking method* to these digital signals.

3.3 Experimental system for pressure diameter test

To validate the elastic modulus, $|E_\theta^h(f_{ac})|$, measured by the *phased tracking method*, the elastic modulus of the tube was also evaluated by testing the relationship between internal pressure and external diameter. The measurement system is illustrated in Fig. 4. In this experiment, the relationship between internal pressure and external diameter was tested by generating the change in internal pressure by compressing a rubber balloon using an actuator. Internal pressure and external diameter were measured by a pressure transducer (NEC 9E02-P16) and a laser line gauge (KEYENCE VG-035), respectively. From the relationship obtained, the elastic modulus in the circumferential direction was evaluated by the incremental elastic modulus, E_{inc}, defined as follows:[28]

$$E_{inc} = \frac{3}{2} \frac{r_0^2 r_e}{r_e^2 - r_0^2} \frac{\Delta p(t)}{\Delta r_e(t)}, \tag{3.1}$$

where r_e and r_0 are the external radius and the inner radius at the end of diastole, respectively, and $\Delta r_e(t)$ is the change in external radius from r_e.

As with eq. (2.11), eq. (3.1) is rewritten by describing $\Delta r_e(t) = \Delta r_{e0} \cdot e^{j(2\pi f_{ac}t - \psi)}$ and $\Delta p(t) = \Delta p_0 \cdot e^{j2\pi f_{ac}t}$ as follows:

$$E_{inc}(f_{ac}) = \frac{3}{2} \frac{r_0^2 r_e}{r_e^2 - r_0^2} \frac{\Delta p_0}{\Delta r_{e0}} \cdot e^{j\psi}, \tag{3.2}$$

where Δr_{e0} is the amplitude of the change in external diameter.

4. Basic Experiments Using a Silicone Rubber Tube

4.1 Estimation of viscoelasticity with ultrasound

Figure 5 shows the B-mode image of a silicone rubber tube. By setting the ultrasonic beam at the position shown in Fig. 5, the M-mode image was obtained as shown in Fig. 6(a). Figure 6(b) shows the measured internal pressure. From Fig. 6(b), it was found that the change in internal pressure at the measurement position can be generated by remotely applied actuation. By setting two points, A and B, along the ultrasonic beam at a time $t = 0$ in the M-mode image, the velocities, $v_A(t)$ and $v_B(t)$, of these points were obtained by the *phased tracking method* as shown in Figs. 6(c) and 6(d). The change in the thickness, $\Delta h(t)$, of the anterior wall was obtained by integrating the difference between these two velocities. In Fig. 6(e), a minute change in the thickness of
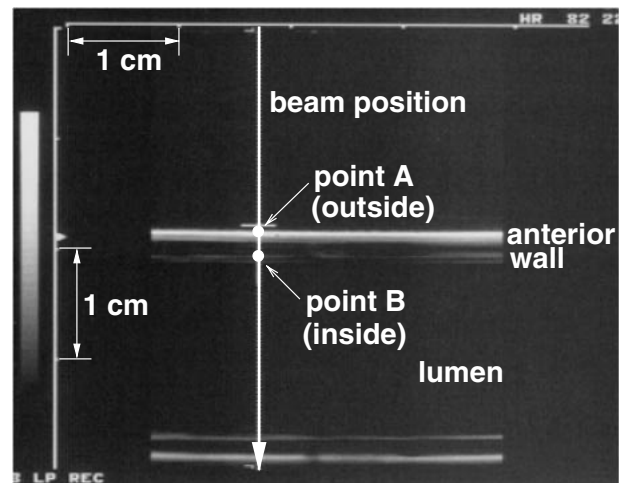

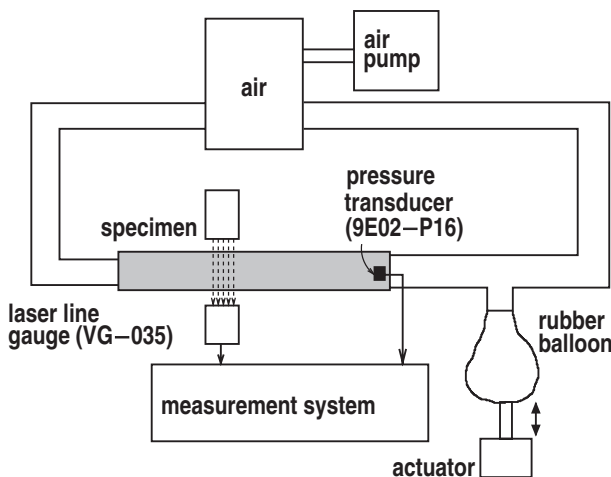Fig. 5.   B-mode image of a silicone rubber tube.

Fig. 4.   Experimental system employed for testing the relationship between the internal pressure, $\Delta p(t)$, and the external diameter, $2\Delta r_e(t)$.
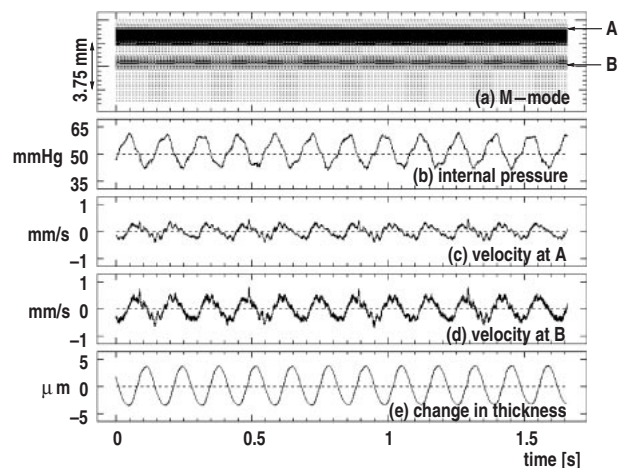

Fig. 6.   (a) M-mode image of the silicone rubber tube. (b) Internal pressure. (c) Velocity, $v_A(t)$, of point A. (d) Velocity, $v_B(t)$, of point B. (e) Change in thickness, $\Delta h(t)$, of the anterior wall (actuation frequency of 7.5 Hz).
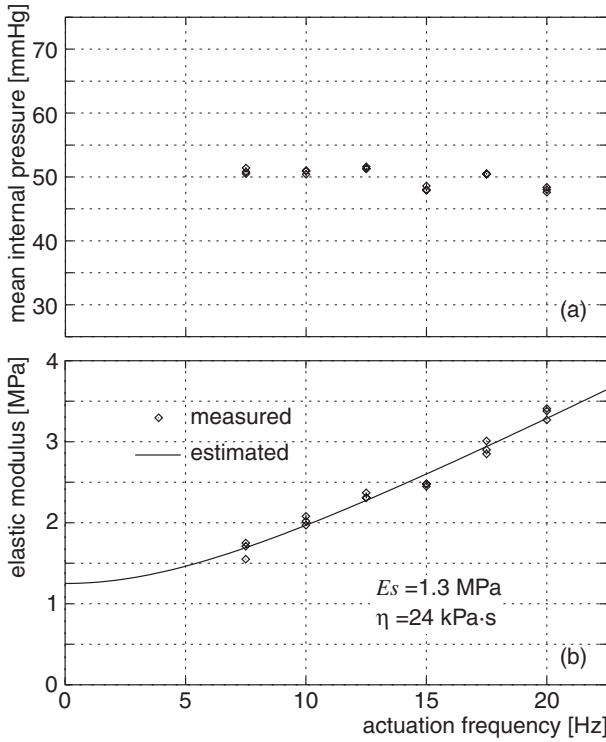
Fig. 7. (a) Mean internal pressure. (b) Elastic moduli, $|E_\theta^h(f_{ac})|$, measured at each actuation frequency, f_{ac}, using ultrasound (plot), and the estimated Voigt model (solid curve).
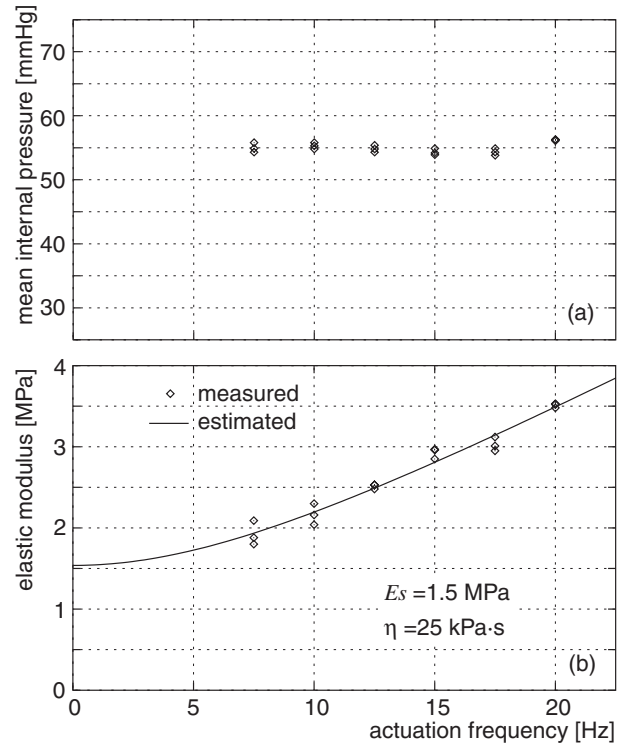

Fig. 8. (a) Mean internal pressure. (b) Elastic moduli, $|E_{inc}(f_{ac})|$, measured at each actuation frequency, f_{ac}, using the laser line gauge (plot), and the estimated Voigt model (solid curve).

less than $10\,\mu\text{m}$ was measured at an actuation frequency of $7.5\,\text{Hz}$. Furthermore, the change in internal pressure, $\Delta p(t)$, at other frequencies can be generated by changing the actuation frequency, f_{ac}. In this study, changes in wall thickness, $\Delta h(t)$, and internal pressure, $\Delta p(t)$, were measured at multiple frequencies from $7.5\,\text{Hz}$ to $20\,\text{Hz}$. To obtain the amplitude of the change in wall thickness, Δh_0, and that of the change in internal pressure, Δp_0, at the actuation frequency, f_{ac}, the Fourier transform was applied to those waveforms. The elastic modulus, $|E_\theta^h(f_{ac})|$, at each actuation frequency, which is shown by diamonds in Fig. 7, was obtained from the estimated Δh_0 and Δp_0. The static elastic modulus, E_s, and the viscosity constant, η, were estimated as $E_s = 1.3\,\text{MPa}$ and $\eta = 25\,\text{kPa·s}$, respectively, by minimizing the mean squared difference between eq. (2.14) and $|E_\theta^h(f_{ac})|$ measured by ultrasound. In Fig. 7, the estimated Voigt model is shown by a solid curve.

4.2 Comparison with results obtained using a laser line gauge

The static elastic modulus and the viscosity constant measured by ultrasound as shown in Fig. 7 were validated by measurements using the laser line gauge.

In Fig. 8, the elastic modulus, $|E_{inc}(f_{ac})|$, which was obtained by measuring the change in internal pressure, $\Delta p(t)$, and the change in external diameter, $2\Delta r_e(t)$, using a pressure transducer and a laser line gauge, respectively, is shown by diamonds. The static elastic modulus, E_s, and the viscosity constant, η, were estimated to be $E_s = 1.5\,\text{MPa}$ and $\eta = 25\,\text{kPa·s}$, respectively, by minimizing the mean squared difference between eq. (2.14) and $|E_{inc}(f_{ac})|$ measured using a laser line gauge.

The static elastic modulus, E_s, and the viscosity constant, η, measured by ultrasound ($E_s = 1.3\,\text{MPa}$, $\eta = 25\,\text{kPa·s}$) were in good agreement with those obtained by the laser line gauge ($E_s = 1.5\,\text{MPa}$, $\eta = 25\,\text{kPa·s}$). From these results, it is found that the viscoelasticity of the silicone rubber tube can be estimated using the ultrasonic *phased tracking method* combined with remote actuation.

4.3 Comparison with the static elastic modulus measured by the static experiment

The measured static elastic modulus, E_s, by ultrasound was also validated by comparing it with E_s obtained by the different static experiment.

In this experiment, the change in internal pressure was increased using an air pump. Figure 9 shows the relationship between the change in wall thickness measured by ultra-
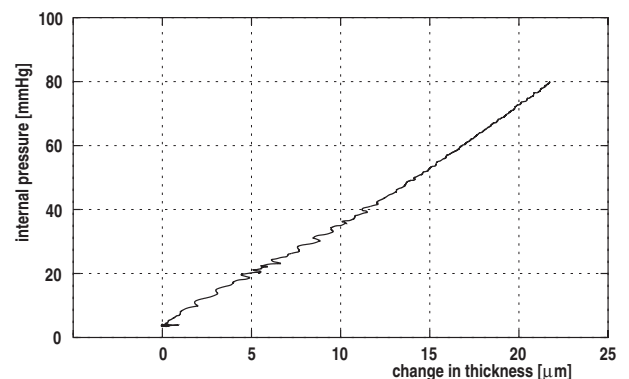

Fig. 9. Relationship between the change in wall thickness, $\Delta h(t)$, and the change in internal pressure, $\Delta p(t)$.
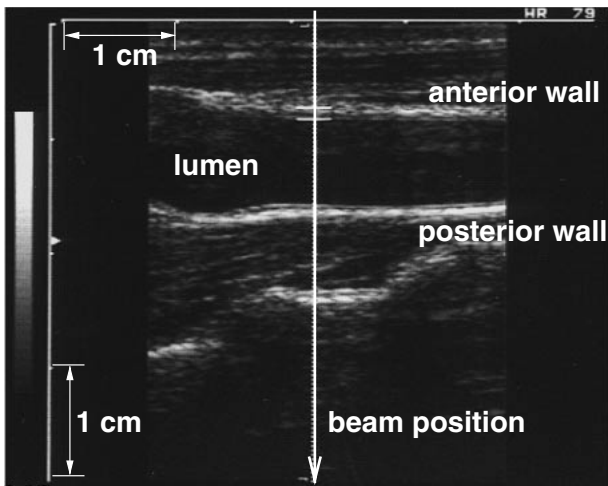
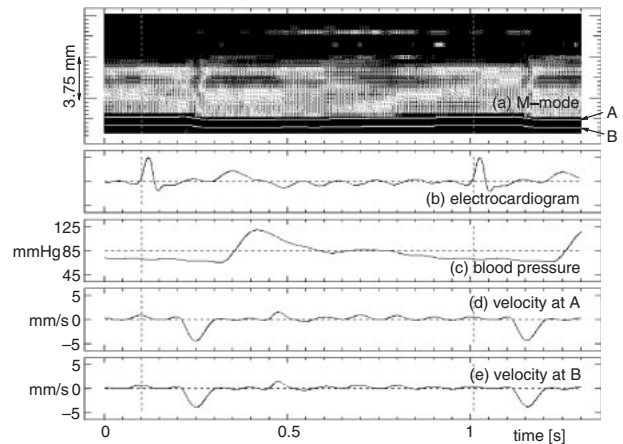Fig. 10.   B-mode image of a human carotid artery (29-year-old male).

Fig. 11.   (a) M-mode image of a human carotid artery. (b) Electrocardiogram. (c) Blood pressure measured at the radial artery using an applanation tonometer. (d) Velocity of the intimal side. (e) Velocity of the adventitial side.

sound and the change in internal pressure measured by the pressure transducer. Because of the nonlinearity in the stress-strain relationship shown in Fig. 9, the static elastic modulus, E_s, changes with the pressure level (1.2 MPa at 30 mmHg, 1.5 MPa at 50 mmHg, 1.6 MPa at 70 mmHg). In §4.1 and §4.2, $|E_\theta^h(f_{ac})|$ and $|E_{inc}(f_{ac})|$ were measured at a mean internal pressure of 50 mmHg. At a pressure of 50 mmHg, the static elastic modulus, E_s, was determined to be 1.5 MPa by this static experiment, and the value agreed well with that obtained by ultrasound (1.3 MPa).

5.   *In vivo* Measurement at a Human Carotid Artery

In *in vivo* experiments, remote actuation was applied from the skin surface at the brachial artery using an actuator, and the change in wall thickness due to the remote actuation was measured at the carotid artery.

Figure 10 shows the B-mode image of the carotid artery of a 29-year-old male. By setting the ultrasonic beam at the position shown in Fig. 10, the M-mode image was obtained as shown in Fig. 11(a). Figure 11(c) shows the blood pressure measured at the radial artery with an applanation tonometer (COLIN JENTOW7700). By setting two points, A (intimal side) and B (adventitial side), along the ultrasonic beam at the R-wave of the electrocardiogram shown in Fig. 11(b), the velocities, $v_A(t)$ and $v_B(t)$, of these points were obtained by the *phased tracking method* as shown in Figs. 11(d) and 11(e), respectively. In Figs. 11(d) and 11(e), there are velocity components caused by remote actuation (10 Hz). Furthermore, changes in internal pressure, $\Delta p(t)$, at other frequencies were generated by changing the actuation frequency, f_{ac}. In this *in vivo* measurement, changes in wall thickness, $\Delta h(t)$, and internal pressure, $\Delta p(t)$, were measured at frequencies of 7.5 Hz, 10 Hz, and 12.5 Hz.

In cardiac systole, there are velocity components caused by the heartbeat, and it is difficult to discriminate those from the velocity component caused by remote actuation. Therefore, in this study, the amplitude of velocity components caused by remote actuation was measured in cardiac diastole. Figures 12(1), 12(2), and 12(3) show internal pressures and velocities at the intimal and adventitial sides approximately 0.6 s after the R-wave of the electrocardiogram at actuation frequencies of 7.5 Hz, 10 Hz and 12.5 Hz,
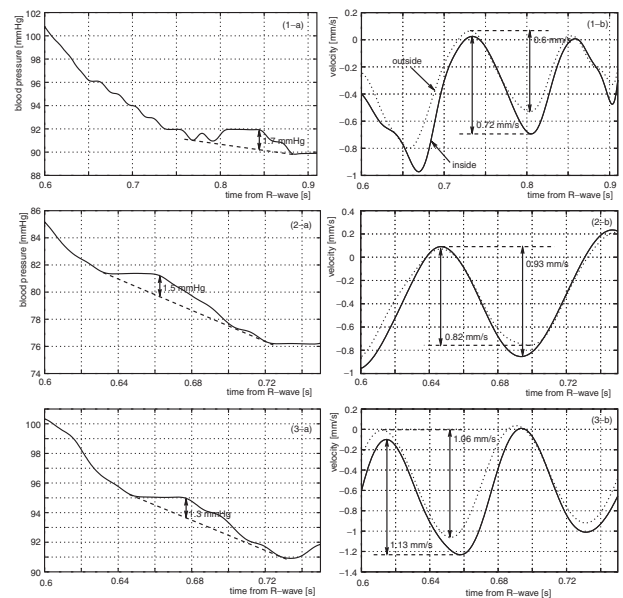
Fig. 12.   Blood pressure and velocity after 0.6 s from the R-wave of electrocardiogram. (1) 7.5 Hz. (2) 10 Hz. (3) 12.5 Hz. (a) Blood pressure. (b) Velocities at the intimal side and the adventitial side.

respectively. In Fig. 12, it is shown that the amplitude of velocity at the intimal side is larger than that at the adventitial side. The changes in wall thickness were calculated from the differences between the amplitudes of velocities at the intimal side and the adventitial side, which can be measured from Figs. 12(1-b), 12(2-b), and 12(3-b). From the amplitudes, Δp_0 and Δh_0, of the change in internal pressure and the change in wall thickness measured from Fig. 12, the elastic modulus, $|E_\theta^h(f_{ac})|$, at each actuation frequency is obtained and plotted as a function of actuation frequency, f_{ac}, as shown in Fig. 13. In Fig. 13, it is shown that the elastic modulus, $|E_\theta^h(f_{ac})|$, increases with actuation frequency, f_{ac}. From the measured $|E_\theta^h(f_{ac})|$, the static elastic modulus, E_s, and the viscosity constant, η, were estimated to be 100 kPa and 3.0 kPa·s, respectively.

The relationship between the mean internal pressure and the elastic modulus of the human carotid artery is reported in
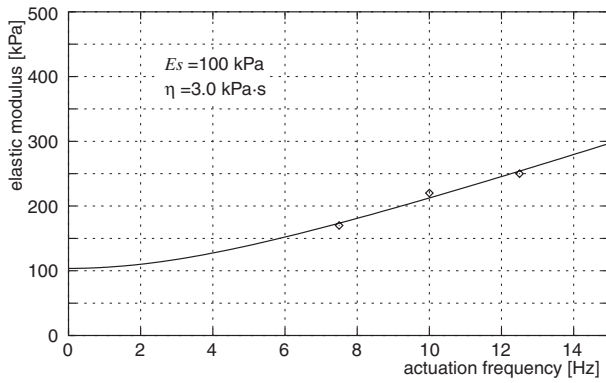
Fig. 13. Elastic moduli, $|E_\theta^h(f_{ac})|$, of a carotid artery measured at multiple frequencies (plot), and the estimated Voigt model (solid curve).

the literature.[29] At a pressure of about 120 mmHg, which corresponds to the systolic pressure, the elastic modulus is about 1.4 MPa. In diastole (blood pressure: about 60 mmHg), it is reported that the elastic modulus has a similar value (about 200 kPa) in comparison with that measured in this paper during diastole. Furthermore, the viscosity constant is reported to be about 5 kPa·s. The viscosity constant measured by the proposed method is in good agreement with that reported in literature.

From these results, it is found that the viscoelasticity of the arterial wall can be measured with transcutaneous ultrasound using remote actuation.

6. Conclusions

In this study, basic experiments were performed for the assessment of viscoelastic properties of the arterial wall. If the wall is viscoelastic, the elastic modulus is changed by the frequency of the applied stress. To investigate the frequency characteristic of the elastic modulus, it is necessary to generate changes in internal pressure at multiple frequencies. By measuring the resultant minute change in wall thickness by our *phased tracking method*, the frequency characteristic of the elastic modulus was obtained. We then assume the Voigt model as a viscoelastic model of the wall, and the static elastic modulus and the viscosity constant were obtained from the elastic moduli measured at multiple actuation frequencies. Such a method for the noninvasive measurement of the viscoelasticity has potential for the characterization of tissues in the arterial wall.

1) S. Glagov, E. Weisenberg, C. K. Zarins, R. Stankunavicius and G. J. Kolettis: New Engl. J. Med. **316** (1987) 1371.
2) R. T. Lee, A. J. Grodzinsky, E. H. Frank, R. D. Kamm and F. J. Schoen: Circulation **83** (1991) 1764.
3) H. M. Loree, A. J. Grodzinsky, S. Y. Park, L. J. Gibson and R. T. Lee: J. Biomech. **27** (1994) 195.
4) P. C. G. Simons, A. Algra, M. L. Bots, D. E. Grobbee and Y. van der Graaf: Circulation **100** (1999) 951.
5) E. Falk, P. K. Shah and V. Fuster: Circulation **92** (1995) 657.
6) M. J. Davies: Circulation **94** (1996) 2013.
7) J. Golledge, R. M. Greenhalgh and A. H. Davies: Stroke **31** (2000) 774.
8) A. P. G. Hoeks, C. J. Ruissen, P. Hick and R. S. Reneman: Ultrasound Med. Biol. **11** (1985) 51.
9) T. Länne, H. Stale, H. Bengtsson, D. Gustafsson, D. Bergqvist, B. Sonesson, H. Lecerof and P. Dahl: Ultrasound Med. Biol. **18** (1992) 451.
10) A. P. G. Hoeks, X. Di, P. J. Brands and R. S. Reneman: Ultrasound Med. Biol. **19** (1993) 727.
11) P. J. Brands, A. P. Hoeks, M. C. Rutten and R. S. Reneman: Ultrasound Med. Biol. **22** (1996) 895.
12) J. M. Meinders, P. J. Brands, J. M. Willigers, L. Kornet and A. P. G. Hoeks: Ultrasound Med. Biol. **27** (2001) 785.
13) D. H. Bergel: J. Physiol. **156** (1961) 445.
14) L. H. Peterson, R. E. Jensen and J. Parnell: Circ. Res. **8** (1960) 622.
15) K. Hayashi, H. Handa, S. Nagasawa, A. Okumura and K. Moritake: J. Biomech. **13** (1980) 175.
16) H. Kanai, M. Sato, Y. Koiwa and N. Chubachi: IEEE Trans. Ultrason. Ferroelectr. Freq. Control **43** (1996) 791.
17) H. Kanai, H. Hasegawa, N. Chubachi, Y. Koiwa and M. Tanaka: IEEE Trans. Ultrason. Ferroelectr. Freq. Control **44** (1997) 752.
18) H. Hasegawa, H. Kanai, N. Chubachi and Y. Koiwa: Electron. Lett. **33** (1997) 340.
19) H. Hasegawa, H. Kanai, N. Chubachi and Y. Koiwa: Jpn. J. Med. Ultrason. **24** (1997) 851.
20) H. Hasegawa, H. Kanai, N. Hoshimiya, N. Chubachi and Y. Koiwa: Jpn. J. Appl. Phys. **37** (1998) 3101.
21) H. Kanai, K. Sugimura, Y. Koiwa and Y. Tsukahara: Electron. Lett. **35** (1999) 949.
22) H. Hasegawa, H. Kanai, N. Hoshimiya and Y. Koiwa: Jpn. J. Appl. Phys. **39** (2000) 3257.
23) H. Hasegawa, H. Kanai, N. Hoshimiya and Y. Koiwa: Jpn. J. Med. Ultrason. **28** (2001) J3.
24) H. Hasegawa, H. Kanai and Y. Koiwa: Jpn. J. Appl. Phys. **41** (2002) 3563.
25) H. Kanai, H. Hasegawa, M. Ichiki, F. Tezuka and Y. Koiwa: Circulation **107** (2003) 3018.
26) H. Hasegawa, H. Kanai, Y. Koiwa and J. P. Butler: Jpn. J. Appl. Phys. **42** (2003) 3255.
27) D. J. Patel, J. S. Janicki and R. N. Vaishnav: Circ. Res. **32** (1973) 93.
28) D. H. Bergel: J. Physiol. **156** (1961) 445.
29) B. M. Learoyd and G. Taylor: Circ. Res. **18** (1966) 278.